Instabilities in the boundary layer over a permeable, compliant wall

Franck Pluvinage, Azeddine Kourta, and Alessandro Bottaro

Citation: Physics of Fluids (1994-present) **26**, 084103 (2014); doi: 10.1063/1.4892086
View online: http://dx.doi.org/10.1063/1.4892086
View Table of Contents: http://scitation.aip.org/content/aip/journal/pof2/26/8?ver=pdfcov
Published by the AIP Publishing

PHYSICS OF FLUIDS **26**, 084103 (2014)

Instabilities in the boundary layer over a permeable, compliant wall

Franck Pluvinage,[1,a)] Azeddine Kourta,[1] and Alessandro Bottaro[2]
[1]*Univ. Orléans, INSA-CVL, PRISME, EA 4229, F45072 Orléans, France*
[2]*DICCA, Scuola Politecnica, Università di Genova, 1 via Montallegro, 16145 Genova, Italy*

(Received 1 April 2014; accepted 13 July 2014; published online 11 August 2014)

Local linear stability of swept and unswept incompressible boundary layers developing over compliant, fluid-saturated, porous plates is considered in the limit of small permeability. The analysis is meant to yield preliminary indications on the possible stabilization induced on the flow's hydrodynamic and hydroelastic modes by poroelastic media, such as those occurring in many natural and technological settings. As far as hydrodynamic modes are concerned, the main stabilizing effect is that of compliance, which however couples weakly to low-frequency crossflow modes. Permeability plays a damping role on hydroelastic modes, which here take the form of travelling wave flutter instabilities. The passive control of instabilities through poroelastic coatings specifically designed to selectively exploit the effect of compliance and/or permeability is a subject worthy of future research efforts. © *2014 AIP Publishing LLC*. [http://dx.doi.org/10.1063/1.4892086]

I. INTRODUCTION

Fluid flow above and throughout poroelastic media occurs in a variety of technological and natural applications, including, in order of decreasing length scales, vegetation canopies,[1,2] birds' covert feathers,[3,4] tennis balls,[5,6] endothelial glycocalyx of blood vessels,[7,8] cytoplasm of living cells,[9] and carbon-nanototubes-based flow sensors.[10,11] The use of flexible, permeable media to bound a flowing fluid is also acquiring momentum in applications related to both sensing[12–14] and manipulating[15–22] near-wall transitional and turbulent structures. Such media often take the form of dense bundles of pillars, hinged at a rigid base and free to vibrate under the forcing provided by the fluid, so that elastic potential energy can be easily transferred to the fluid and back. Effective field equations for media constituted by ordered pillars and disordered carpets have been recently proposed by Gopinath and Mahadevan[23] on the basis of homogenization theory.

Here the focus is on stability issues for swept and unswept boundary layers over thin plates which are both flexible and porous, the goal being to find trends on linear stability boundaries upon variation of parameters like the elastic modulus of the plate or its permeability. Previous related studies consider either the stability of channel flows bounded by one or two porous walls,[24–29] or the stability of channel and boundary layer flows past flexible walls.[30–34] In the first configuration (porous wall) destabilization of Tollmien-Schlichting (TS) modes is found, even in the presence of walls which are very weakly permeable. Conversely, the second case (compliant wall) is associated to a reduction of the region in parameter space where hydrodynamic modes are excited (for both TS and crossflow - CF - instabilities, as will be shown here), but causes the appearance of rapidly amplifying wall modes (in the remainder of the paper, such modes are called FISI, for "flow induced surface instabilities"). To the best of the authors' knowledge, there are no studies on the stability of incompressible flows over a poroelastic medium saturated by a fluid, and the present work represents a first step in this direction, albeit in the limit of small permeability.

[a)]Electronic mail: franck.pluvinage@univ-orleans.fr

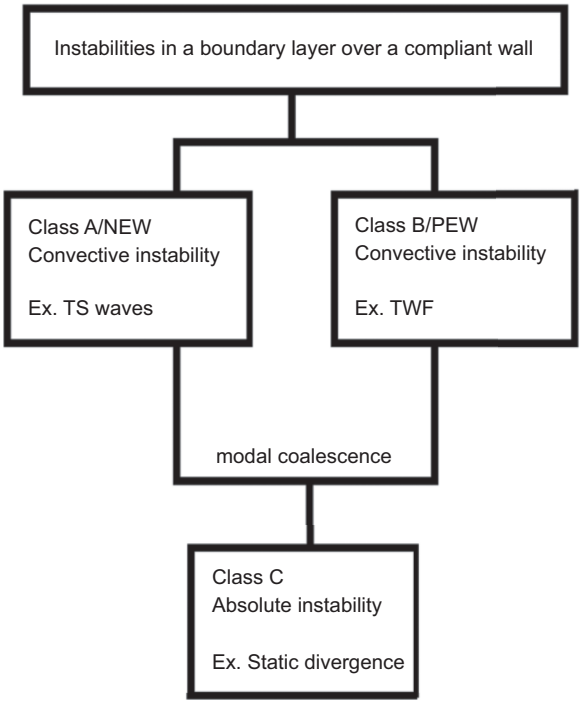

FIG. 1. Schematic of classification of fluid-solid instabilities.

The different instabilities which might be observed in a boundary layer over a compliant wall are summarized in Fig. 1. The original classification scheme, due to Benjamin[35] and Landahl,[36] divides the modes into three categories based upon the response of the wave to irreversible energy transfer to and from the compliant surface. Class A waves, also called "negative energy waves" (NEW) in the plasma physics community, are destabilized by dissipation within the coating, i.e., increased dissipation of energy in the wall yields an increase in wave amplitude. A typical example of a class A wave is the viscous TS instability; Class B waves (also known as PEW for "positive energy waves") are stabilized by an increase in the viscous dissipation in the coating or the medium. An example of such an instability is the mode known as "travelling wave flutter" (TWF, one of the FISI). When PEW and NEW co-exist, there is the possibility of modal interaction and coalescence. Modal coalescence between different branches of solutions and the emergence of waves with zero group velocities are necessary conditions for there to be an absolute instability. Class C modes are absolute instabilities for which hydrodynamic forces cause a unidirectional transfer of energy to the wall. For example, the coalescence between TS waves (class A) and TWF (class B) yields the so-called transitional mode (class C), identified theoretically by Sen and Arora.[37] A well-known class C mode is static divergence, a FISI which can be observed in the presence of high shear at the wall and/or wall damping.[38] Static divergence has a very small phase speed and manifests itself as a periodic series of humps and valleys at the surface, as documented experimentally by Gad-el-Hak[39] in 1986; ten years later, Gad-el-Hak[40] states that "in a physical experiment it is rather difficult to distinguish between the static-divergence waves and the transitional ones." In the present work static divergence modes are never amplified, and FISI are thus always of the travelling-wave type.

The objective of this work is to ascertain if and how a small amount of wall permeability has an effect on the onset of hydrodynamic and hydroelastic instabilities. We model the wall as a Kramer-type compliant surface,[41] using classical thin-plate theory;[42] the fact that it is porous and permeated by the fluid is rendered by a simple Darcy's law, as described in Sec. II. Section III addresses the effects of the permeability of the plate on TS and CF modes, whereas Sec. IV presents results on the impact of compliance on stability, including FISI. The combined effect of porosity and compliance is addressed in Sec. V, while concluding remarks are given in Sec. VI.

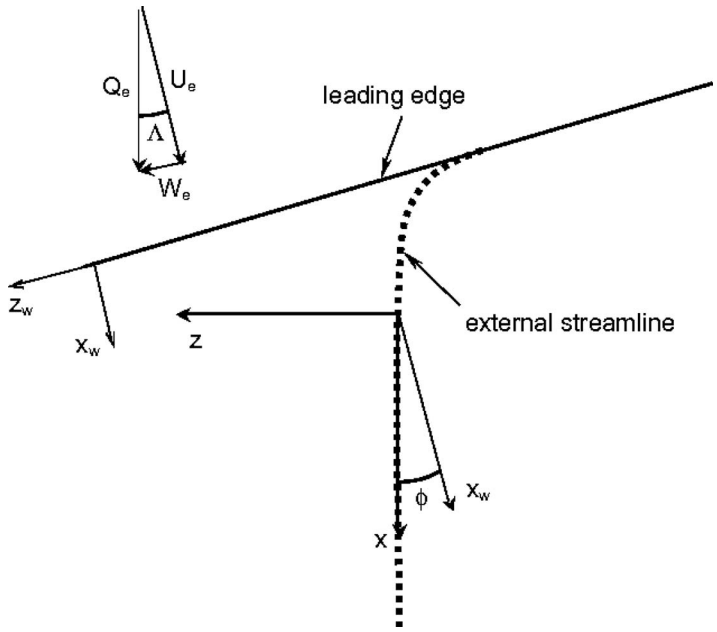

FIG. 2. Sketch of the coordinate systems for the boundary layer over a swept wing.

II. THE MODEL

The incompressible boundary layer which forms over a swept plate is modeled using the family of similarity solutions given by Cooke.[43] This model relies on the specification of two parameters: one, m, describes the intensity of the pressure gradient, and the second, the sweep angle Λ, provides a relation between chordwise and spanwise components of the velocity. The configuration illustrated in Fig. 2 shows the swept plate seen from above: the wing coordinate system is described by x_w and z_w, aligned, respectively, along the plate's chord and the plate's spanwise sense, with y the wall-normal direction. The corresponding velocity components within the boundary layer are denoted by U_w, W_w, and V. The velocity at the boundary layer edge (denoted in the following by using subscript "e") at any position x_w is defined by $U_e = C{x_w}^m$, with C a suitable constant, and W_e = constant. A similarity solution can be found by introducing the characteristic boundary layer scale $\delta(x_w) = \left(\frac{2}{m+1}\frac{\nu x_w}{U_e}\right)^{1/2}$ and defining the variable $\xi = y/\delta(x_w)$. Then, if a streamfunction is defined in the form $\psi = \left(\frac{2}{m+1}\nu x_w U_e\right)^{1/2} f(\xi)$, continuity is satisfied directly and $U_w = U_e f'(\xi)$ (apostrophe denoting derivation with respect to the independent variable). Assuming $W_w = W_e\, g(\xi)$, the momentum equations yield the system:

$$f''' + ff'' + \frac{2m}{m+1}(1 - f'^2) = 0, \qquad g'' + fg' = 0 \tag{1}$$

with

$$f(0) = f'(0) = g(0) = 0 \quad \text{and} \quad f'(\infty) = g(\infty) = 1. \tag{2}$$

It is customary to study stability in the frame of reference of the external streamline. Let ϕ be the angle between the frame aligned with the external potential flow streamline and the wing coordinate system; some distance from the leading edge it is appropriate to take $\phi \approx \Lambda$ (cf. Fig. 2), so that the velocity components along x and z are given by

$$U(\xi) = Q_e[f'(\xi)\cos^2\Lambda + g(\xi)\sin^2\Lambda], \tag{3}$$

$$W(\xi) = Q_e[g(\xi) - f'(\xi)]\cos\Lambda\sin\Lambda. \tag{4}$$

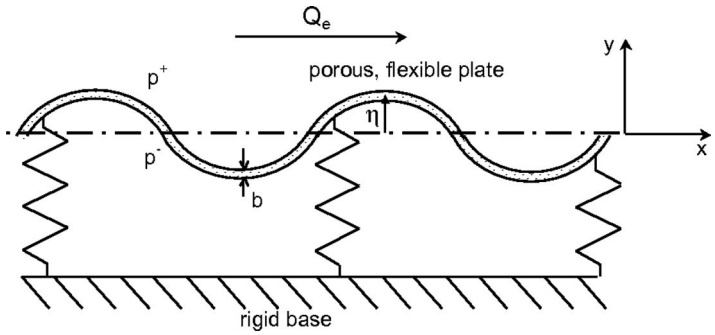

FIG. 3. Sketch of the problem considered; figure not to scale.

The parallel flow assumption is now enforced, and infinitesimal disturbances (u, v, w, p) are superimposed to a locally parallel base state $(U, 0, W, P)$. By using as independent variables the physical coordinates (x, y, z) and time t, the disturbance equations in dimensionless form read:

$$\frac{\partial u}{\partial t} + U\frac{\partial u}{\partial x} + vU' + W\frac{\partial u}{\partial z} = -\frac{\partial p}{\partial x} + \frac{1}{Re}\Delta u, \tag{5}$$

$$\frac{\partial v}{\partial t} + U\frac{\partial v}{\partial x} + W\frac{\partial v}{\partial z} = -\frac{\partial p}{\partial y} + \frac{1}{Re}\Delta v, \tag{6}$$

$$\frac{\partial w}{\partial t} + U\frac{\partial w}{\partial x} + vW' + W\frac{\partial w}{\partial z} = -\frac{\partial p}{\partial z} + \frac{1}{Re}\Delta w, \tag{7}$$

$$\frac{\partial u}{\partial x} + \frac{\partial v}{\partial y} + \frac{\partial w}{\partial z} = 0, \tag{8}$$

where Δ is the Laplacian operator and the Reynolds number is defined as $Re = \dfrac{Q_e\delta}{\nu}$; Q_e is the velocity scale, $\delta = \delta(l)$ is the length scale (with l a reference distance along the chordwise direction), ρQ_e^2 is the pressure scale, with ρ the density of the fluid and ν its kinematic viscosity.

The boundary layer is assumed to develop above an isotropic plate of uniform thickness b, whose midplane coincides with the plane $y = 0$; the plate is attached to a rigid, impermeable base through regularly arranged stubs which behave like springs, and the same fluid permeates both the regions above and below the plate. Following Carpenter and Davis,[44] we assume that, under the effect of the mean pressure gradient and/or mean viscous stresses, the wall is maintained horizontal.

A small perpendicular displacement $\eta(x, z, t)$ of the plate from its rest position is assumed, caused by the load exerted by the medium which flows above it (Fig. 3).

Provided that $\eta \ll b$ and that the wavelength of the plate's flexural motion is much larger than b, η satisfies the (dimensional) bending wave equation:

$$\rho_p b\frac{\partial^2\eta}{\partial t^2} + d\frac{\partial\eta}{\partial t} + B\nabla_2^4\eta - T\nabla_2^2\eta + \kappa\eta = -[p], \tag{9}$$

where ρ_p is the plate's density, d is a damping coefficient per unit area, $B = \dfrac{Eb^3}{12(1-\nu_p^2)}$ is the bending stiffness of the plate (with E Young modulus and ν_p Poisson ratio), $\nabla_2^4 = \nabla_2^2\nabla_2^2$ is the biharmonic operator, with $\nabla_2^2 = \dfrac{\partial^2}{\partial x^2} + \dfrac{\partial^2}{\partial z^2}$, T is the longitudinal tension per unit width, κ is the spring stiffness per unit area, and $[p] = p^+ - p^-$ denotes the jump in perturbation pressure across the plate. Without loss of generality, we assume that the fluid pressure within the confined region is uniform, so that $[p] = p^+(x, \eta, y, t)$; in the following, superscript $+$ will be dropped.

The flexible plate is further assumed to be weakly porous, with isotropic permeability k_D sufficiently small for the seepage velocity of the unperturbed state to either vanish or be of such a

reduced magnitude that the parallel flow approximation remains tenable. The Darcy's flux along y for a rigid plate can be expressed as

$$\langle v \rangle = -\frac{k_D}{\rho \nu}\frac{\partial p}{\partial y} = -\frac{k_D}{\rho \nu}\frac{[p]}{b}; \tag{10}$$

it is related to the actual velocity of the fluid in the interstitial space via the porosity of the material. Moderate to large values of the permeability and anisotropic effects are out of the scope of the present paper; the case could be treated with effective field theories of poroelastic media such as those outlined by Whitaker[45] or Mei and Vernescu.[46] In such a case, the base velocity field on top of which disturbances are imposed must include three components of the velocity through the fluid-infiltrated porous plate, with the permeability being a tensor. Some progress along these lines is reported by Hill and Straughan[27] and Tilton and Cortelezzi[29] for the case of rigid, isotropic, porous block(s) delimiting a channel, in the limit of negligible inertial effects within the porous block(s). A different approach is described by Battiato[47] for both porous and poroelastic composites confining the flow in a channel. Her poroelastic formulation considers small displacements of the medium, so that the analysis of the flow and the mechanics of the elastic medium can be decoupled. The analyses by Hill and Straughan, Tilton and Cortelezzi, and Battiato eventually resort to using a Brinkman model in the porous region adjacent the bulk fluid, plus interface conditions. The definition of such conditions is still subject of debate: Beavers and Joseph[48] have proposed to use an interfacial slip velocity; Ochoa-Tapia and Whitaker[49,50] adopt continuous tangential velocity and discontinuous shear stress (this is the condition used also by Tilton and Cortelezzi[28,29]); Cieszko and Kubik[51] argue that both tangential velocity and shear stress are discontinuous; conversely for Vafai and Kim[52] these same quantities must be continuous (both Hill and Straughan, and Battiato follow this line). This unclear scenario stems from the fact that near the interface microscopic velocity and pressure fields vary rapidly over length scales of the order of the pore size, whereas a formulation of the porous matrix based on Darcy's or Brinkmann's laws requires a matching across the interface based on spatially averaged quantities.[23]

Accounting for both plate's deflection and flow through the pores, the boundary conditions for the perturbation velocity components at $y = \eta$ are

$$u = 0, \quad v = \frac{\partial \eta}{\partial t} - \frac{k_D}{\rho \nu b}p, \quad w = 0. \tag{11}$$

To place the numerical boundary at $y = 0$, we use a first order Taylor expansion in η, thus replacing the first condition above with $u + \eta U' = 0$, the other two remaining unchanged. The boundary conditions and the plate's equation can be rendered dimensionless by adopting appropriate scale. In particular, we scale η with δ and further define:

$$\chi^* = \frac{\rho_p Q_e b}{\rho \nu}, \quad d^* = \frac{d}{\rho Q_e}, \quad B^* = \frac{B Q_e}{\rho \nu^3}, \quad T^* = \frac{T}{\rho \nu Q_e}, \quad \kappa^* = \frac{\kappa \nu}{\rho Q_e^3}. \tag{12}$$

The set of plate's parameters is independent of δ, i.e., we assume that Q_e, ρ, and ν are fixed, and that Re can increase simply with the observer moving along the plate in the chordwise sense, so that l and δ vary.

All components of the disturbance field, (u, v, w, p) and η, are assumed to behave like normal modes of the form:

$$exp(i\alpha x + i\beta z + \sigma t),$$

with α and β real wavenumbers, $k^2 = \alpha^2 + \beta^2$, and σ the complex amplification factor; equations plus boundary conditions are modified accordingly. The dimensionless equation for the plate's displacement thus becomes (dropping asterisks):

$$\left(\frac{\chi}{Re}\sigma^2 + d\sigma + \frac{B}{Re^3}k^4 + \frac{T}{Re}k^2 + \kappa Re\right)\eta = -p, \tag{13}$$

and the disturbance boundary conditions at $y = 0$ are

$$u + \eta U' = 0, \quad v = \sigma\eta - ap, \quad w = 0, \tag{14}$$

where the dimensionless permeability coefficient $a = \dfrac{k_D Q_e}{\nu b}$ arises from the nondimensionalisation; a is the product of the Reynolds number Re, times the Darcy number $Da = \dfrac{k_D}{b^2}$, times the ratio between the plate's thickness b and the boundary layer scale δ. Re-arranging the equations above it is easy to find three suitable boundary conditions for the fluid which apply at $y = 0$:

$$\frac{\chi}{Re}\sigma(v + ap) + d(v + ap) - \frac{1}{U'Re}\left(\frac{B}{Re^2}k^4 + Tk^2 + \kappa Re^2\right)u = -p, \tag{15}$$

$$\sigma u + U'(v + ap) = 0, \tag{16}$$

$$w = 0. \tag{17}$$

At the outer edge of the boundary layer, disturbances are taken to vanish by enforcing asymptotic boundary conditions; numerical tests have been carried out to ensure that the outermost grid point is placed sufficiently far from $y = 0$ for the solution to be unaffected by this choice. The code developed solves for the disturbance equations in primitive form; it is based on a classical Chebyshev collocation approach similar to that used in previous studies[34,53,54] and it has been extensively validated against results for both rigid and compliant surfaces.[30,31,55–58] The local approximation used here implies a separation of scale between the mean flow and the disturbance field, with the consequence that the results for low α ($\alpha < 0.05$ for the Blasius case) must be interpreted with caution.

To set ideas, the parameters used by Carpenter and Garrad (meant to reproduce and explain Kramer's[41] experimental results in water) for a wall which is untensioned can be employed, i.e., $Q_e = 18$ m/s, $\rho = 1025$ kg/m^3, $\rho_p = 945$ kg/m^3, $\nu = 1.37 \times 10^{-6}$ m^2/s, $b = 2 \times 10^{-3}$ m, and $\nu_p = 0.5$. This choice yields: $\chi = 24226$, $B = 6.08 \times 10^6\ E$, $\kappa = 5.27 \times 10^{-11}\ E$ (following Carpenter and Garrad who considered springs/stubs of length equal to 1 mm), $a = 6.57 \times 10^9\ k_D$, with both Young modulus E and permeability k_D expressed in SI units. To limit the number of available parameters, the viscous damping d is set equal to zero. An increase in elastic modulus represents an increase in wall rigidity and typical values of E do not exceed 10^5 Pa for soft polyvinyl chloride (PVC), 6×10^5 Pa for silicon rubber, 2×10^9 Pa for polypropylene, and 2×10^{11} Pa for steel. An increase in k_D means that seepage through the pores is enhanced for a given pressure gradient. Values of water permeability depend on the structure and porosity of the material; k_D is of order 10^{-14} m^2 for granite; 8×10^{-8} m^2 for nickel foametal, 10^{-8} m$^2 \div 10^{-6}$ m^2 for polyester textiles and ceramic foams. These numbers yield coefficients a in the range $10^{-4} \div 10^4$; because of the arguments presented earlier we will limit our parametric search to values of a up to one.

Finally, assuming that the chordwise length of the plate is of the order of the meter, we will explore values of the Reynolds number $Re = \dfrac{Q_e \delta}{\nu}$ up to 5000, covering adequately the region where the first instabilities appear, for both swept and unswept plates.

III. EFFECT OF PLATE'S PERMEABILITY ON THE INSTABILITIES DEVELOPING OVER A SWEPT PLATE

To have a point of reference, we first focus on the case for which the crossflow velocity is maximized, i.e., $\Lambda = 45^\circ$. Neutral stability boundaries for $\beta = 0$ and for $\beta = 0.4$ are displayed in Fig. 4, both values of the spanwise wavenumbers coinciding with those of largest amplification for the instability mode which is observed.

In the first instance, TS instabilities are amplified over a range of α's which shrinks with increasing m. As expected, adverse pressure gradient enhances destabilization. In the second case, low-frequency crossflow modes are preferentially excited, with the range of unstable values of α which increases with m. The critical Reynolds number for CF modes reaches its lower limit for m equal to 0.4 and does not decrease upon further enhancement of the pressure gradient.

The results are summarized in Fig. 5; for adverse pressure gradients, the CF disturbances become unstable at values of Re well above the critical values Re_c of TS modes.

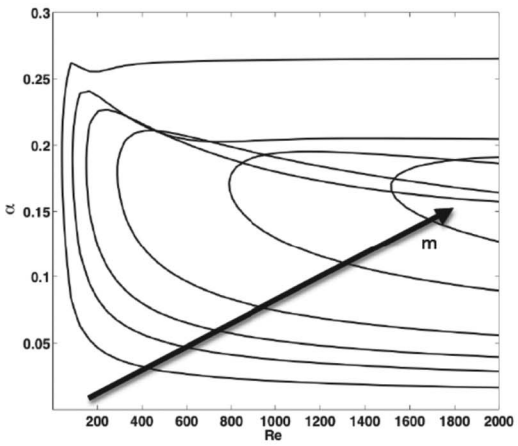

(a)Neutral curves for TS modes over a swept plate for $\beta = 0$ and increasing values of m, as indicated by the arrow $(m = -0.09; -0.07; -0.045; 0; 0.1; 0.2)$.

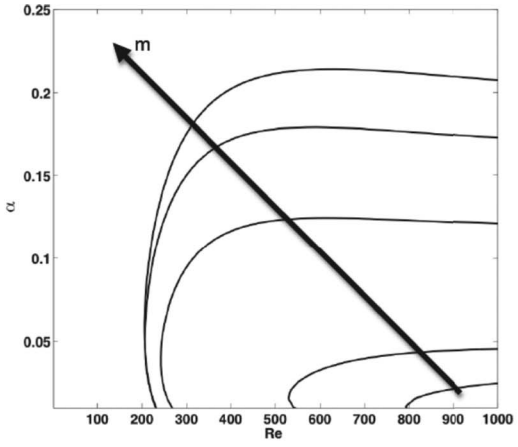

(b)Neutral curves for CF modes over a swept plate for $\beta = 0.4$ and increasing values of m, as indicated by the arrow $(m = 0.03; 0.05; 0.2; 0.4; 0.6)$.

FIG. 4. Linear stability results for accelerated/decelerated boundary layers over a plate swept at $\Lambda = 45^\circ$.

On the contrary, for m exceeding 0.05 the reverse is true, and low-frequency crossflow modes define the onset of transition. These same modes have already been computed by Mack,[55] and our results match his (cf. his Figure 13.5). Figure 5 provides also an overview on the effect of a weak permeability of the plate on the onset of TS and CF modes (dotted and dashed lines, respectively). Permeability is destabilizing in both cases and, interestingly, it is observed to have a larger effect on the *Re*-threshold of TS modes. This same influence of permeability on TS modes has already been reported by Chang *et al.*,[26] Hill and Straughan, and Tilton and Cortelezzi[28] for the channel

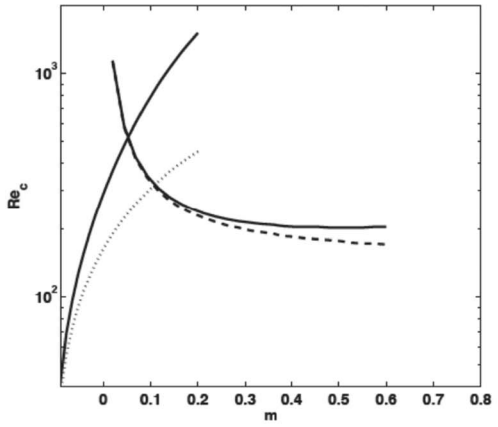

(a)Critical Reynolds number for the flow over a swept plate. Solid lines: TS and CF modes for impermeable wall ($\beta = 0$ and $\beta = 0.4$, respectively). Dotted line: TS instability threshold for a permeable wall with $a = 0.1$; dashed line: CF threshold for $a = 1$.

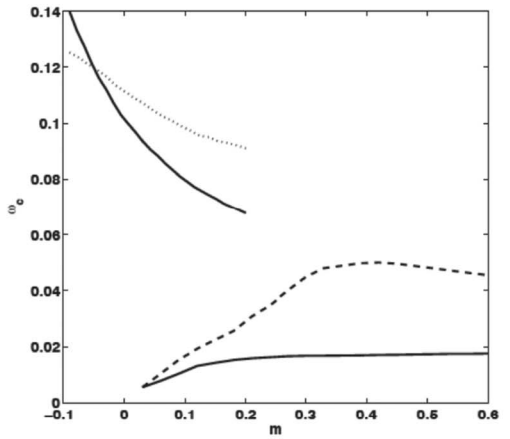

(b)Critical frequency for the flow over a swept plate. Same symbols as in frame (a).

FIG. 5. Critical conditions for TS and CF modes developing in the boundary layer over a plate swept at $\Lambda = 45^\circ$, for both impermeable and weakly permeable walls.

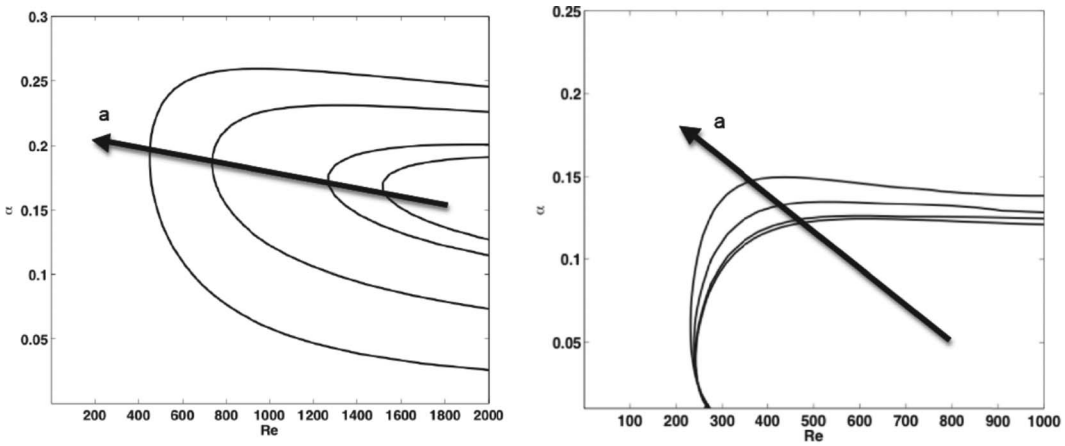

(a)Neutral curves for TS modes at $\beta = 0$ $(a = 0; 0.01; 0.05; 0.1)$.

(b)Neutral curves for CF modes at $\beta = 0.4$ $(a = 0; 0.1; 0.5; 1)$.

FIG. 6. Effect of permeability on the marginal stability curves for the flow past a swept wing ($m = 0.2$, $\Lambda = 45^\circ$).

flow case, on the basis of different theoretical models. It is further seen here that weak permeability of the plate tends to increase the critical frequency at the onset of the instability, for both TS and CF modes.

The marginal stability curves for varying a's are displayed in Fig. 6. For both instability modes, permeability enlarges the streamwise wavenumber's range of unstable modes, and the effect is clearly more pronounced for the case of TS modes. The mode shapes of representative disturbances are plotted in Fig. 7 and the effect of permeability on the shape of either TS or CF perturbations is minor.

IV. EFFECT OF PLATE'S COMPLIANCE

The influence of compliance on two-dimensional TS waves in a Blasius boundary layer has been addressed before, cf. Allen[58] and Al Musleh and Frendi.[59] The results given here are meant

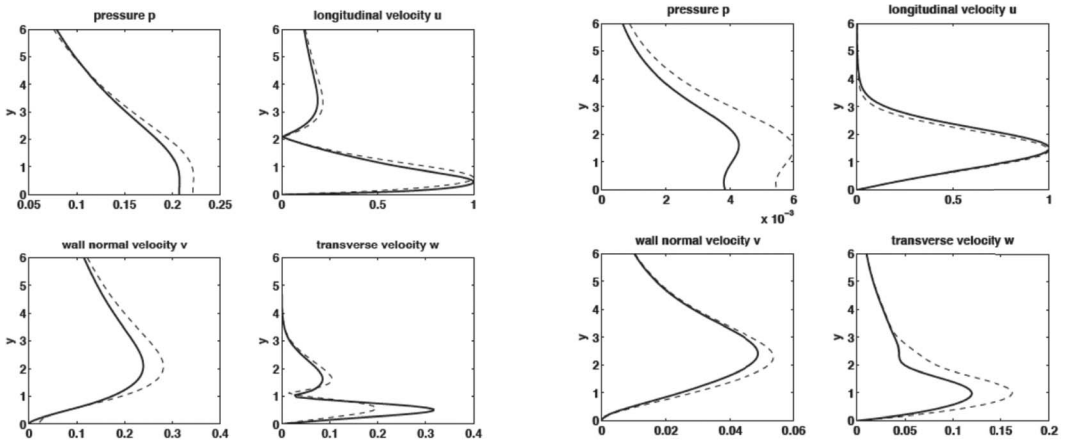

(a)TS mode; Plain line : $a = 0$, $Re = 1520$ and $\alpha = 0.169$; Dashed line: $a = 0.1$, $Re = 450$ and $\alpha = 0.191$

(b)CF mode; Plain line : $a = 0$, $Re = 242$ and $\alpha = 0.038$; Dashed line: $a = 1$, $Re = 231$ and $\alpha = 0.058$

FIG. 7. Perturbation profiles at the critical points of the curves in Figure 6.

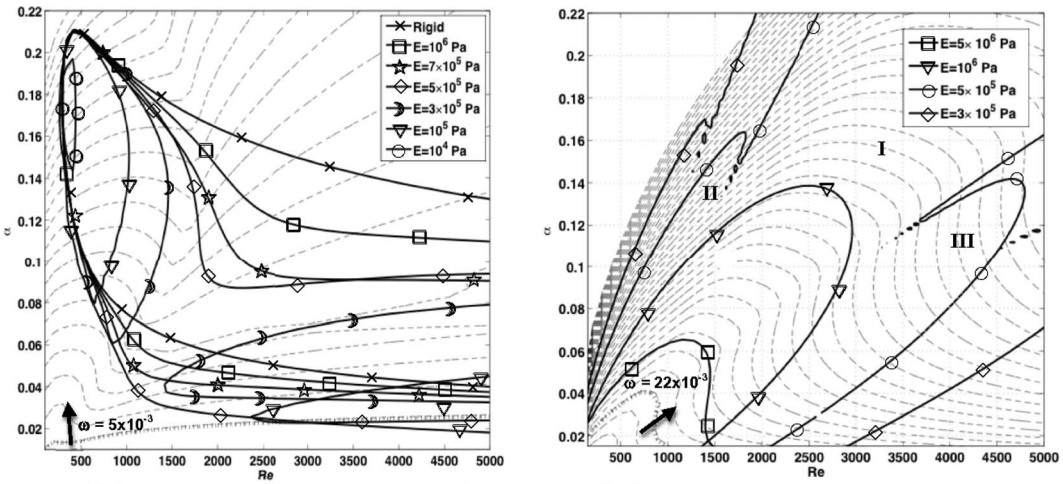

(a)Dashed lines: frequency isolines for $E = 3 \times 10^5$, thus $B = 1.8 \times 10^{12}$, with increasing ω indicated by the arrow in steps equal to 4×10^{-3}.

(b)Dashed lines: frequency isovalues for $E = 3 \times 10^5$, thus $B = 1.8 \times 10^{12}$, with ω increasing from the reference, thicker, dashed line in steps of 5×10^{-3}.

FIG. 8. Variation of TS (a) and FISI (b) neutral curves for varying wall elastic modulus E on a Blasius boundary layer ($\phi = 0^\circ$, $m = 0$, $\beta = 0$).

to be used as a basis on which to later assess the consequence of the plate's permeability (Sec. V). Figure 8(a) illustrates the outcome of varying the Young modulus E and demonstrates that rendering the plate softer reduces the size of the unstable region, eventually causing it to split into two separate parts, with the leftmost one which disappears for E below 10^4Pa. It is thus recovered the known result that compliance stabilizes TS waves, while exciting surface modes as shown in Fig. 8(b). The unstable eigen-domain in this case can be divided into three portions, of increasing size with the wall softening. The central region (denoted as I in Fig. 8(b)) displays larger growth rates compared to the uppermost (II) and lowermost (III) regions. Carpenter and Garrad[30,31] indicate that the mode arising in this central region is travelling wave flutter, with a phase speed close to the free-stream velocity; our results provide a value of the phase velocity always comprised between 0.8 and 1 in region I. The classification of the modes in the other two regions with respect to the scheme of Fig. 1 has not been indicated in Refs. 30 and 31; we observe here that disturbances in regions II and III are wall-based modes travelling faster than the external stream (phase speed consistently in the range [1, 1.6]). We thus believe that they are convective PEW, like those in region I. The disturbance shapes in regions II and III resemble one another, and differ from those of the main region I, cf. Fig. 9. All the mode shapes are essentially unaffected by the presence of permeability.

When the boundary layer is swept, compliance acts as illustrated in Figs. 10 and 11. With the parameters chosen, the threshold for the appearance of crossflow vortices is $Re = 250$, $\alpha = 0.05$, and $\beta = 0.4$. Figure 10 shows that this threshold is not influenced by compliance, even for the case of soft walls because of the weak coupling that an elastic boundary can have with quasi-steady crossflow modes. When the wall becomes essentially a membrane which offers no resistance to bending loads (i.e., when Young's modulus is very small) a disturbance of relatively high phase velocity emerges at larger values of α (cf. Fig. 10(a)). The elasticity of the wall, at low frequencies and low values of the streamwise wavenumber, manifests itself with a reduction in the range of unstable α's, and the occurrence of FISI which are preferentially z-independent at onset (Fig. 10(b)). The neutral curves in Fig. 10(b) display a merger between the travelling wave flutter and the crossflow mode, which is anticipated (in Re terms) for softer walls. These results are in qualitative agreement with those obtained by Carpenter and Thomas[60] for the case of the rotating disk boundary layer, highlighting the similarities between the two configurations even in the presence of a compliant wall. The main

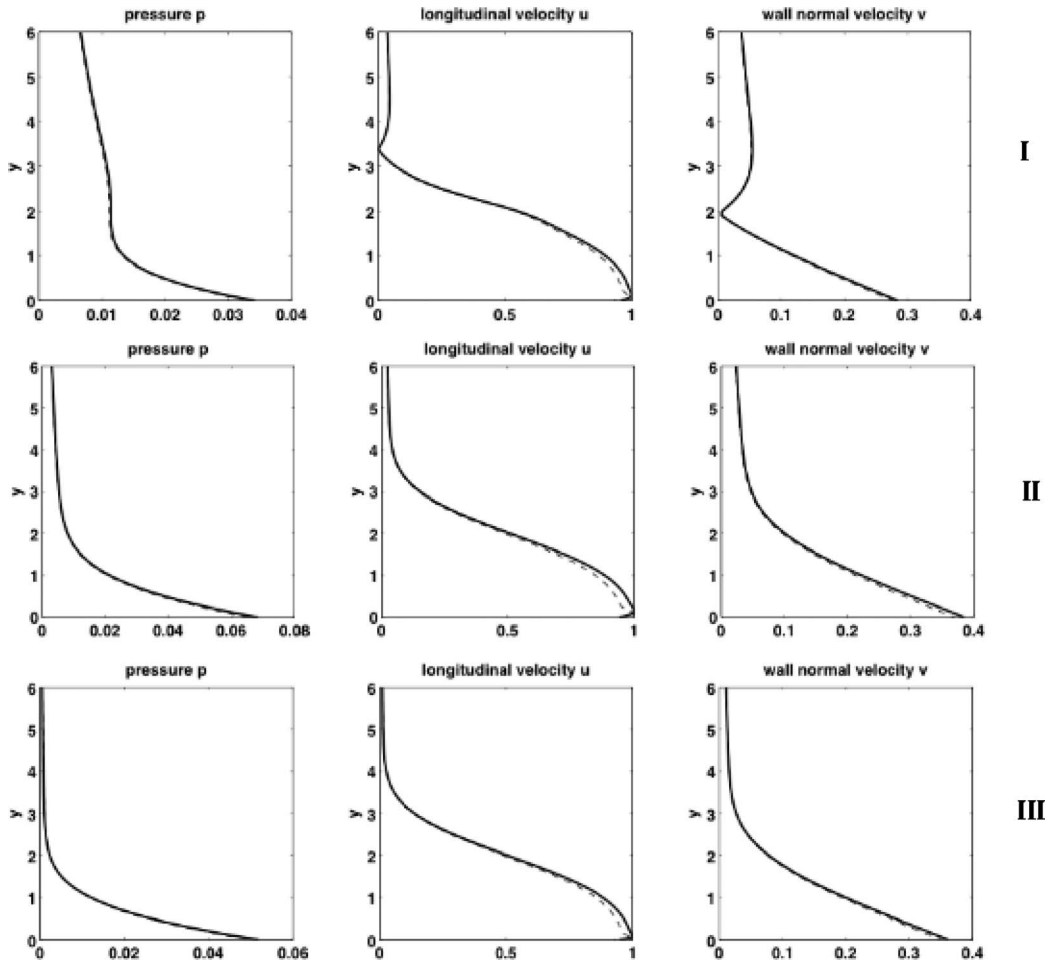

FIG. 9. TWF modes shapes in region I (at Re=2500), II (at Re=1200), and III (at Re=4000). Plain lines: $a = 0$; dashed lines: $a = 1$ (other parameters: $\alpha = 0.12$, $E = 5 \times 10^5\ Pa$, thus $B = 3.04 \times 10^{12}$, $\phi = 0$, $m = 0$, $\beta = 0$).

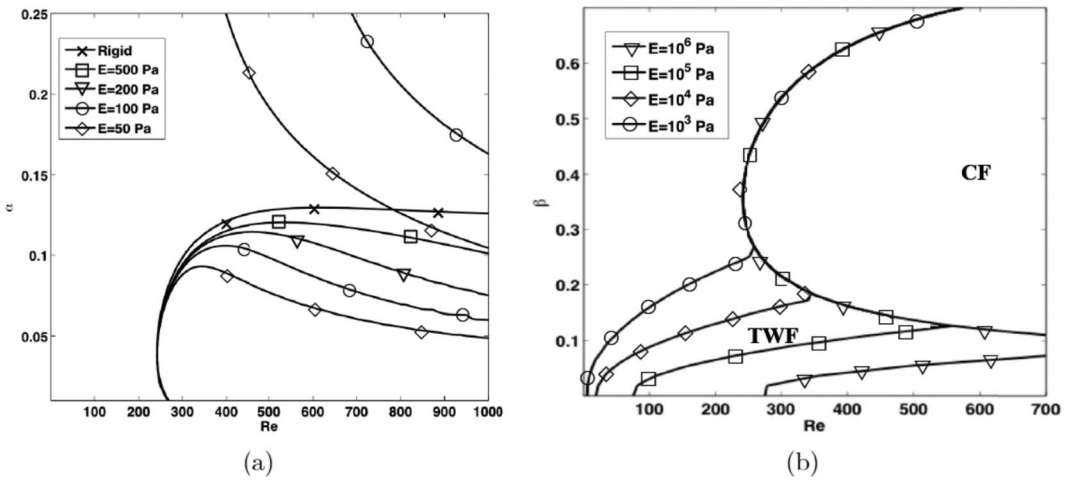

FIG. 10. Variation of CF neutral curves for decreasing wall elastic modulus E in (a) the $Re - \alpha$ plane for $\beta = 0.4$, and (b) the $Re - \beta$ plane for $\alpha = 0.05$ ($\phi = 45^\circ$, $m = 0.2$). To set ideas a value $E = 100\ Pa$ corresponds to $B = 6.08 \times 10^8$.

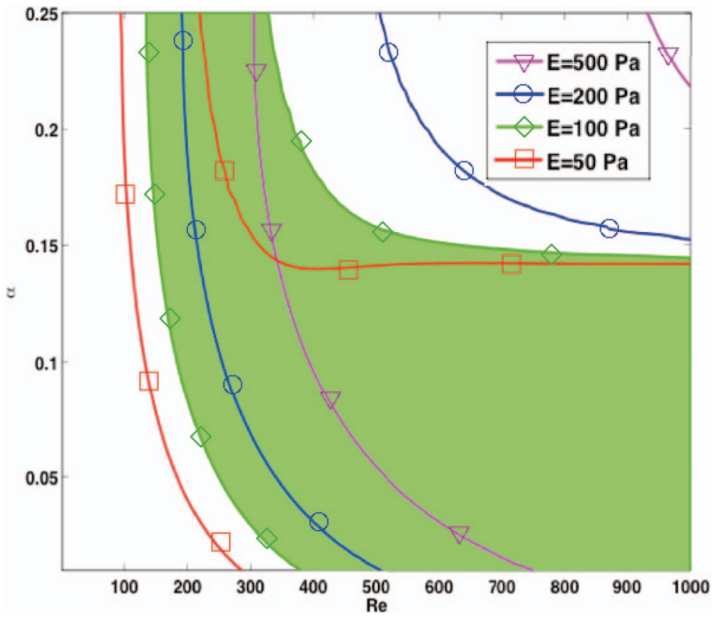

FIG. 11. Effect of varying elastic modulus on TWF for a swept boundary layer ($\phi = 45^\circ$, $m = 0.2$, $\beta = 0.4$). The unstable region for $E = 100\ Pa$ is shaded for clarity.

difference is that, at fixed α, here Re_c for the onset of TWF decreases monotonically; conversely, in the case of the rotating disk the behavior of Re_c is not monotonic with E, a consequence of Coriolis effects.[60,61] For decreasing values of E the TWF appears at progressively smaller Re's, covering a progressively larger β range, eventually overruling the crossflow vortices even at the lower β ($\beta_c = 0.4$) for which the CF mode appears (as displayed in Fig. 11). The moduli of the critical CF and TWF mode shapes in the limit of very soft plate ($E = 100\ Pa$) are shown in Fig. 12; the consequence of weak permeability is most noticeable on the surface-based hydroelastic mode.

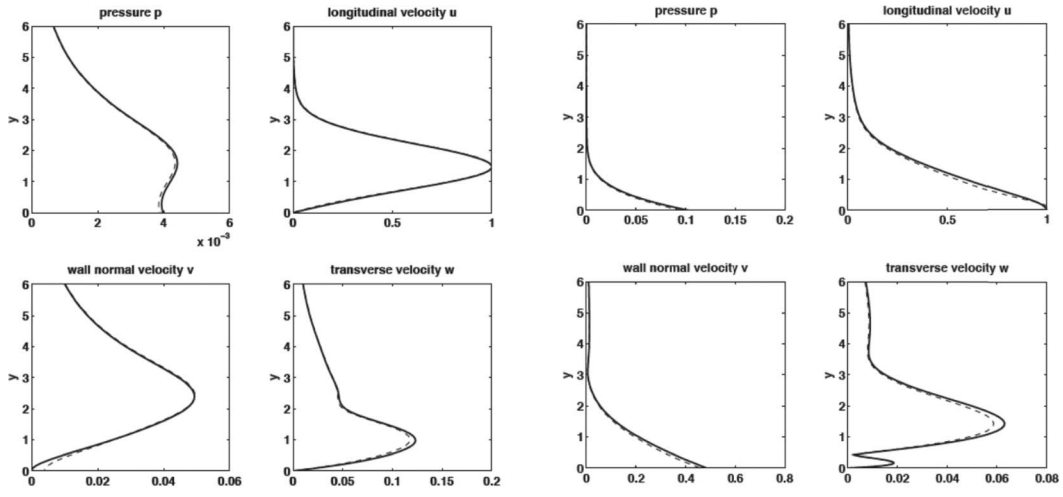

(a)CF mode at $Re = 242$ and $\alpha = 0.04$; plain line: $a = 0$; dashed line: $a = 1$.

(b)TWF mode at $Re = 140$ and $\alpha = 0.25$; plain line: $a = 0$; dashed line: $a = 1$.

FIG. 12. Most unstable CF and TWF mode shapes ($E = 100\ Pa$, thus $B = 6.08 \times 10^8$, $\phi = 45^\circ$, $m = 0.2$, $\beta = 0.4$).

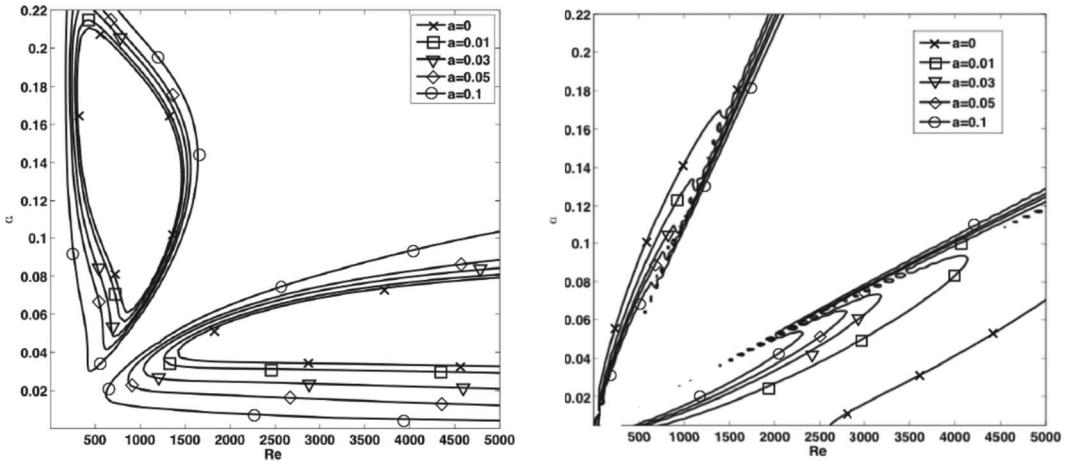

FIG. 13. TS (a) and FISI (b) neutral curves as function of the permeability coefficient a for a Blasius boundary layer ($\phi = 0^\circ$, $m = 0$, $\beta = 0$, $E = 3 \times 10^5\ Pa$, thus $B = 1.8 \times 10^{12}$).

V. POROELASTIC PLATE

A. Effect of permeability on the Blasius boundary layer over a compliant wall

The fact of rendering the plate permeable enhances the TS instability (cf. Fig. 13(a)) and this is borne, in analogy to the action of wall damping on class A NEW, by the plate's boundary condition

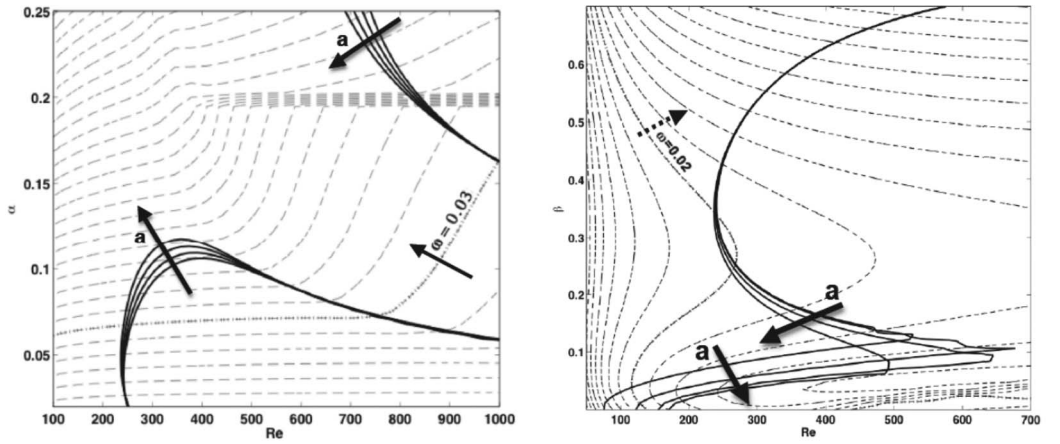

(a)Plain lines: CF neutral curves with varying permeability a ($E = 100\ Pa$, thus $B = 6.08 \times 10^8$, $\beta = 0.4$, $a = 0; 0.2; 0.4; 0.6$). Dashed lines: frequency isovalues for $a = 0$ with growing direction indicated by the arrow and interval between successive isolines equal to 5×10^{-3}. The horizontal dashed lines around $\alpha = 0.2$ for Re larger than about 400 are an artefact of the plotting routine, at the interface between two modes with strong differences in frequency

(b)Plain lines: CF and TWF neutral curves with varying permeability a ($E = 10^5\ Pa$, thus $B = 6.08 \times 10^{11}$, $\alpha = 0.05$, $a = 0; 0.02; 0.1; 0.2$). Dashed lines: frequency isovalues for $a = 0$ with growing direction indicated by the arrow and interval between successive isolines equal to 1×10^{-3}.

FIG. 14. Neutral curves on a swept plate boundary layer ($\phi = 45^\circ$, $m = 0.2$).

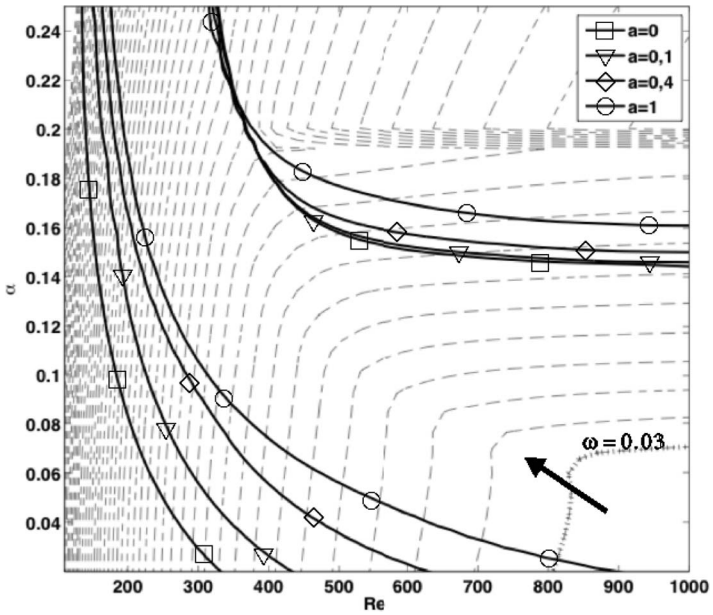

FIG. 15. Plain lines: TWF neutral curves with varying permeability a on a swept plate boundary layer. Dashed lines: frequency isovalues for $a = 0$ with growing direction indicated by the arrow and interval between successive isolines equal to 5×10^{-3} ($\phi = 45°$, $m = 0.2$, $\beta = 0.4$, $E = 100\ Pa$, thus $B = 6.08 \times 10^8$).

for the vertical velocity v: the increase of seepage through the pores is responsible for reduced plate's oscillations. Conversely, the effect on FISI is stabilizing: the size of region I is mildly reduced by permeability, but that of regions II and III is significantly so, as shown in Fig. 13(b). This reinforces the argument that the modes present in regions II and III are class B PEW, with permeability playing the role of substrate damping. It would be interesting to develop a model allowing the study of larger values of k_D, possibly including anisotropic effect, to evaluate whether the onset of FISI could be delayed even more.

B. Effect of permeability on crossflow and hydroelastic waves

An example of the result of permeability on the crossflow instability is illustrated in Fig. 14: both high and low frequency CF modes seem but very mildly sensitive to permeable damping, and the critical Reynolds number is essentially unaffected in the range of a's tested. The benefits of permeable damping on FISI appear to be more pronounced (cf. Fig. 14(b)) and the critical value of Re roughly doubles when going from $a = 0$ to $a = 0.2$.

When the wall is very soft (the case $E = 100$ Pa is taken as an example in Fig. 15), the effect is qualitatively similar, and the lower branch neutral curve is shifted towards larger Re values, and particularly so for the case of long streamwise waves.

VI. CONCLUSIONS

A temporal, parallel stability analysis has been used to study the instability waves which can develop in the boundary layer over a swept plate which can be compliant and/or permeable to the fluid. The model developed couples thin plate's theory and Darcy's equation, and results in a fictitious wall condition applicable in the limit of small displacement and permeability of the wall. Despite the simplicity of the approach, this paper presents the first indications of how compliance and porosity conjures to destabilize the flow over a swept wing. The results have implications for passive flow control techniques, which are increasingly turning towards poroelastic materials in the quest to mimic the effects observed in biological surfaces.

The presence of a porous substrate at the wall of a boundary layer is summarized in Fig. 5; the effect is destabilizing as far as TS waves are concerned (as already reported previously) but less so for three-dimensional, low-frequency, crossflow modes. The former result is due to the enhanced Reynolds stress near the wall brought about by permeable damping, allowing efficient extraction of energy from the mean flow; the latter stems from the fact that the base flow is unmodified when the permeability coefficient k_D is very small, with an ensuing second order effect on inflectional-driven modes.

As far as compliance is concerned, it is stabilizing for class A Tollmien-Schlichting waves (a result already known[30,31]) but mildly so for low-frequency (class B) crossflow modes, which are impacted upon only when the elastic modulus is very small. When the plate becomes permeable the effect is similar to the rigid case, i.e., very weakly destabilizing.

The upshot of small permeability on FISI is more interesting in light of possible applications: the onset of travelling wave flutter can be significantly postponed in the boundary layer over both swept and unswept plates. This suggests that delaying transition via a suitably designed poroelastic plate is a viable approach to flow control, compliance acting mostly to damp the hydrodynamic modes and porosity mitigating flow-induced surface instabilities, such as TWF. Further studies are called for to strengthen this conclusion, allowing in particular for large, anisotropic permeability, paying however attention not to excite static divergence modes, should the permeable damping influence become too important.

ACKNOWLEDGMENTS

This work started thanks to a Vinci mobility grant awarded to the two senior authors by the "Università Italo-Francese" (project C1-28). A.B. further acknowledges the partial financial support awarded from the EU to Wolf Dynamics through the PelSkin project (Grant No. ACP2-GA-2013-334954-PEL-SKIN).

[1] M. Ghisalberti and H. Nepf, "Shallow flows over a permeable medium: The hydrodynamics of submerged aquatic canopies," Transp. Porous Media **78**, 385–402 (2009).
[2] C. Py, E. de Langre, and B. Moulia, "A frequency lock-in mechanism in the interaction between wind and crop canopies," J. Fluid Mech. **568**, 425–449 (2006).
[3] J. U. Schlüter, "Lift enhancement at low Reynolds numbers using self-activated movable flaps," J. Aircraft **47**, 348–351 (2010).
[4] T. Hanson, *Feathers: The Evolution of a Natural Miracle* (Basic Books, New York, 2011).
[5] R. D. Mehta, "Aerodynamics of sports balls," Annu. Rev. Fluid Mech. **17**(1), 151–189 (1985).
[6] R. D. Mehta, F. Alam, and A. Subic, "Review of tennis ball aerodynamics," Sports Technol. **1**(1), 7–16 (2008).
[7] S. Weinbaum, X. Zhang, Y. Han, H. Vink, and S. C. Cowin, "Mechanotransduction and flow across the endothelial glycocalyx," Proc. Natl. Acad. Sci. U.S.A. **100**(13), 7988–7995 (2003).
[8] J. W. VanTeeffelen, J. Brands, E. S. Stroes, and H. Vink, "Endothelial glycocalyx: Sweet shield of blood vessels," Trends Cardiovasc. Med. **17**, 101–105 (2007).
[9] E. Moeendarbary, L. Valon, M. Fritzsche, A. R. Harris, D. A. Moulding, A. J. Thrasher, E. Stride, L. Mahadevan, and G. T. Charras, "The cytoplasm of living cells behaves as a poroelastic material," Nat. Mater. **12**, 253–261 (2013).
[10] P. Kim and C. M. Lieber, "Nanotube nanotweezers," Science **286**, 2148–2150 (1999).
[11] S. Ghosh, A. K. Sood, and N. Kumar, "Carbon nanotube flow sensors," Science **299**(5609), 1042–1044 (2003).
[12] G. J. Schmitz, C. Brücker, and P. Jacobs, "Manufacture of high-aspect-ratio micro-hair sensor arrays," J. Micromech. Microeng. **15**, 1904 (2005).
[13] Ch. Brücker, D. Bauer, and H. Chaves, "Dynamic response of micro-pillar sensors measuring fluctuating wall-shear-stress," Exp. Fluids **42**, 737–749 (2007).
[14] Y. Z. Liu, H. L. An, J. W. Li, S. H. Zhang, Y. Zhan, and H. L. Zhang, "Selective permeability mechanism of M type K channels," Adv. Mater. Res. **96**, 201–206 (2010).
[15] J. Favier, A. Dauptain, D. Basso, and A. Bottaro, "Passive separation control using a self-adaptive hairy coating," J. Fluid Mech. **627**, 451–483 (2009).
[16] C. Brücker, "Interaction of flexible surface hairs with near-wall turbulence," J. Phys. Condens. Matter **23**, 184120 (2011).
[17] C. Brücker, "Do flexible surface hairs manipulate near-wall turbulence?," *Progress in Turbulence and Wind Energy IV*, Springer Proceedings in Modern Physics Vol. 141 (Springer, Berlin/Heidelberg, 2012), pp. 191–196.
[18] S. Kunze and C. Brücker, "Flow control over an undulating membrane," Exp. Fluids **50**, 747–759 (2011).
[19] S. Kunze and C. Brücker, "Control of vortex shedding on a circular cylinder using self-adaptive hairy-flaps," C. R. Mec. **340**, 41–56 (2012).
[20] C. Brücker and C. Weidner, "Influence of self-adaptive hairy flaps on the stall delay of an airfoil in ramp-up motion," J. Fluids Struct. **47**, 31–40 (2014).

[21] D. Venkataraman and A. Bottaro, "Numerical modeling of flow control on a symmetric aerofoil via a porous, compliant coating," Phys. Fluids **24**, 093601 (2012).
[22] D. Venkataraman, A. Bottaro, and R. Govindarajan, "A minimal model for flow control on an aerofoil using a poro-elastic coating," J. Fluids Struct. **47**, 150–164 (2014).
[23] A. Gopinath and L. Mahadevan, "Elastohydrodynamics of wet bristles, carpets and brushes," Proc. R. Soc. A **467**(2130), 1665–1685 (2011).
[24] A. Goharzadeh, A. Khalili, and B. B. Jørgensen, "Transition layer thickness at a fluid- porous interface," Phys. Fluids **17**, 057102 (2005).
[25] L. M. de Socio, L. Marino, and G. Seminara, "Stability and admittance of a channel flow over a permeable interface," Phys. Fluids **17**(9), 094103 (2005).
[26] M-H. Chang, F. Chen, and B. Straughan, "Instability of Poiseuille flow in a fluid overlying a porous layer," J. Fluid Mech. **564**, 287–303 (2006).
[27] A. A. Hill and B. Straughan, "Poiseuille flow in a fluid overlying a porous medium," J. Fluid Mech. **603**, 137–149 (2008).
[28] N. Tilton and L. Cortelezzi, "The destabilizing effects of wall permeability in channel flows: A linear stability analysis," Phys. Fluids **18**, 051702 (2006).
[29] N. Tilton and L. Cortelezzi, "Linear stability analysis of pressure-driven flows in channels with porous walls," J. Fluid Mech. **604**, 411–445 (2008).
[30] P. W. Carpenter and A. D. Garrad, "The hydrodynamic stability of flow over Kramer-type compliant surfaces. Part 1. Tollmien-Schlichting instabilities," J. Fluid Mech. **155**, 465–510, 9 (1985).
[31] P. W. Carpenter and A. D. Garrad, "The hydrodynamic stability of flow over kramer-type compliant surfaces. Part 2. Flow-induced surface instabilities," J. Fluid Mech. **170**, 199–232 (1986).
[32] P. W. Carpenter and T. J. Pedley, *Flow Past Highly Compliant Boundaries and in Collapsible Tubes: Proceedings of the Uitam Symposium Held at the University of Warwick, United Kingdom, 26-30 March 2001*, Fluid Mechanics and Its Applications Vol. 72 (Kluwer Academic Publisher, Dordrecht, The Netherlands, 2003).
[33] O. Wiplier and U. Ehrenstein, "On the absolute instability in a boundary-layer flow with compliant coatings," Eur. J. Mech. B: Fluids **20**, 127–144 (2001).
[34] J. Hœpffner, A. Bottaro, and J. Favier, "Mechanisms of non-modal energy amplification in channel flow between compliant walls," J. Fluid Mech. **642**, 489–507 (2010).
[35] T. B. Benjamin, "Effects of a flexible boundary on hydrodynamic stability," J. Fluid Mech. **9**, 513–532 (1960).
[36] M. T. Landahl, "On the stability of a laminar incompressible boundary over a flexible surface," J. Fluid Mech. **13**, 609–632 (1962).
[37] P. K. Sen and D. S. Arora, "On the stability of laminar boundary-layer flow over a flat plate with a compliant surface," J. Fluid Mech. **197**, 201–240 (1988).
[38] A. D. Lucey, G. J. Cafolla, and P. W. Carpenter, "Numerical simulation of a boundary-layer flow interacting with a compliant boundary," Lect. Notes Phys. **490**, 406–411 (1997).
[39] M. Gad-el-Hak, "Boundary layer interactions with compliant coatings: An overview," Appl. Mech. Rev. **39**, 511–524 (1986).
[40] M. Gad-el-Hak, "Compliant coatings: A decade of progress," Appl. Mech. Rev. **49**(10), S147–S157 (1996).
[41] M. O. Kramer, "Boundary layer stabilization by distributed damping," J. Am. Soc. Naval Eng. **72**(1), 25–34 (1960).
[42] A. E. H. Love, "On the small free vibrations and deformations of elastic shells," Philos. Trans. R. Soc. (London) **179**, 491–549 (1888).
[43] J. C. Cooke, "The boundary layer of a class of infinite yawed cylinders," Math. Proc. Cambridge Philoso. Soc. **46**, 645–648 (1950).
[44] C. Davies and P. W. Carpenter, "Numerical simulation of the evolution of Tollmien-Schlichting waves over finite compliant panels," J. Fluid Mech. **335**, 361–392 (1997).
[45] S. Whitaker, *The Method of Volume Averaging*, Theory and Applications of Transport in Porous Media (Kluwer Academic Publisher, Dordrecht, The Netherlands, 1999).
[46] C. C. Mei and B. Vernescu, *Homogenization Methods for Multiscale Mechanics* (World Scientific Publishing, Singapore, 2010).
[47] I. Battiato, "Self-similarity in coupled Brinkman/Navier–Stokes flows," J. Fluid Mech. **699**, 94–114 (2012).
[48] G. S. Beavers and D. D. Joseph, "Boundary conditions at a naturally permeable wall," J. Fluid Mech. **30**, 197–207 (1967).
[49] J. A. Ochoa-Tapia and S. Whitaker, "Momentum transfer at the boundary between a porous medium and a homogeneous fluid. I. Theoretical development," Int. J. Heat Mass Transfer **38**, 2635–2646 (1995).
[50] J. A. Ochoa-Tapia and S. Whitaker, "Momentum transfer at the boundary between a porous medium and a homogeneous fluid. II. Comparison with experiment," Int. J. Heat Mass Transfer **38**, 2647–2655 (1995).
[51] M. Cieszko and J. Kubik, "Derivation of matching conditions at the contact surface between fluid-saturated porous solid and bulk fluid," Transp. Porous Media **34**, 319–336 (1999).
[52] K. Vafai and S. J. Kim, "Fluid mechanics of the interface region between a porous medium and a fluid layer: An exact solution," Int. J. Heat Fluid Flow **11**, 254–256 (1990).
[53] A. Guaus, "Analyse linéaire des instabilités dans les écoulements incompressibles à parois courbes compliantes," Ph.D. thesis (Institut de Mécanique des Fluides de Toulouse (IMFT), 2008).
[54] A. Guaus and A. Bottaro, "Instabilities of the flow in a curved channel with compliant walls," Proc. R. Soc. A **463**, 2201–2222 (2007).
[55] L. M. Mack, *Boundary-Layer Stability Theory* (Jet Propulsion Laboratory, California Institute of Technology, Pasadena, 1984).
[56] A. R. Wazzan, T. T. Okamura, and A. M. O. Smith, Spatial and Temporal Stability Charts for the Falkner–Skan Boundary-Layer Profiles, Report No. DAC-67086, McDonnell-Douglas Aircraft Co., Long Beach, CA, 1968.
[57] P. Corbett and A. Bottaro, "Optimal linear growth in swept boundary layers," J. Fluid Mech. **435**, 1–23 (2001).

[58] L. Allen and T. J. Bridges, "Flow past a swept wing with a compliant surface: Stabilizing the attachment-line boundary layer," Stud. Appl. Math. **110**(4), 333–349 (2003).
[59] A. Al Musleh and A. Frendi, "On the effects of a flexible structure on boundary layer stability and transition," ASME J. Fluids Eng. **133**(7), 071103 (2011).
[60] P. W. Carpenter and P. J. Thomas, "Flow over compliant rotating disks," J. Eng. Math. **57**, 303–315 (2007).
[61] A. J. Cooper and P. W. Carpenter, "The stability of rotating-disc boundary-layer flow over a compliant wall. Part 1. Type 1 and 2 instabilities," J. Fluid Mech. **350**, 231–259 (1997).